Journal of Integrative Neuroscience

J. Integr. Neurosci. **2025**; 24(1): 25991
https://doi.org/10.31083/JIN25991

Original Research

Changes in the Parietal Lobe Subregion Volume at Various Stages of Alzheimer's Disease and the Role in Cognitively Normal and Mild Cognitive Impairment Conversion

Fang Lu[1], Qing Ma[2], Cailing Shi[3], Wenjun Yue[1,*]

[1]Department of Radiology, Affiliated Hospital of North Sichuan Medical College, 637000 Nanchong, Sichuan, China
[2]Department of Neurology, North Sichuan Medical College, 637000 Nanchong, Sichuan, China
[3]Department of Radiology, Qionglai Medical Centre Hospital, 611530 Chengdu, Sichuan, China
*Correspondence: ywj820@163.com (Wenjun Yue)

Academic Editor: Rex Jung
Submitted: 3 August 2024 Revised: 21 September 2024 Accepted: 30 September 2024 Published: 21 January 2025

Abstract

Background: Volume alterations in the parietal subregion have received less attention in Alzheimer's disease (AD), and their role in predicting conversion of mild cognitive impairment (MCI) to AD and cognitively normal (CN) to MCI remains unclear. In this study, we aimed to assess the volumetric variation of the parietal subregion at different cognitive stages in AD and to determine the role of parietal subregions in CN and MCI conversion. **Methods**: We included 662 participants from the Alzheimer's Disease Neuroimaging Initiative (ADNI) database, including 228 CN, 221 early MCI (EMCI), 112 late MCI (LMCI), and 101 AD participants. We measured the volume of the parietal subregion based on the Human Brainnetome Atlas (BNA-246) using voxel-based morphometry among individuals at various stages of AD and the progressive and stable individuals in CN and MCI. We then calculated the area under the curve (AUC) of the receiver operating characteristic (ROC) curve to test the ability of parietal subregions to discriminate between different cognitive groups. The Cox proportional hazard model was constructed to determine which specific parietal subregions, alone or in combination, could be used to predict progression from MCI to AD and CN to MCI. Finally, we examined the relationship between the cognitive scores and parietal subregion volume in the diagnostic groups. **Results**: The left inferior parietal lobule (IPL)_6_5 (rostroventral area 39) showed the best ability to discriminate between patients with AD and those with CN (AUC = 0.688). The model consisting of the left IPL_6_4 (caudal area 40) and bilateral IPL_6_5 showed the best combination for predicting the CN progression to MCI. The left IPL_6_1 (caudal area 39) showed the best predictive power in predicting the progression of MCI to AD. Certain subregions of the volume correlated with cognitive scales. **Conclusion**: Subregions of the angular gyrus are essential in the early onset and subsequent development of AD, and early detection of the volume of these regions may be useful in identifying the tendency to develop the disease and its treatment.

Keywords: neuroimaging; mild cognitive impairment; brain subregion; angular gyrus; conversion

1. Introduction

Alzheimer's disease (AD) is the most prominent form of dementia, typically in the elderly, and is linked to the progression of brain volume loss and deterioration of cognitive function with age [1,2]. The progressive deterioration of the cerebrum and cognition constitutes the AD continuum [3]. Within this continuum, the earliest symptomatic phase is designated as mild cognitive impairment (MCI), which has an estimated annual conversion rate of 10–15% to AD [2,4]. The degree of memory and cognition impairment in individuals with MCI is intermediate between that of patients with AD and in individuals who are cognitively normal (CN). However, despite this impairment, their functional capacity remains intact [5,6]. In addition, patients with late MCI (LMCI) exhibit a rapid and pronounced decline in memory, positive cerebrospinal fluid (CSF) biomarkers, elevated white-matter hyperintensities, and distinctive alterations in brain functional connectivity when compared to those with early MCI (EMCI) [7–9]. Therefore, the MCI period represents a pivotal stage in developing neuro biomarkers with the potential to guide diagnostic, therapeutic, and preventive approaches for AD.

Structural magnetic resonance imaging (sMRI) represents a significant non-invasive approach for investigating structural alterations in the brain related to AD and MCI [10]. The involvement of brain regions is distinct at various stages of AD, with grey matter abnormalities initially affecting the hippocampus and amygdala and spreading to the parietal and frontal lobes as the disease progresses [11,12]. The fluctuations in the level of Amyloid beta (Aβ) protein accumulation in various brain regions may reveal this pathological mechanism of structural brain changes [13,14]. Moreover, the trajectories of subregional atrophy exhibit differences even within the same brain throughout AD [15]. Studies have examined the impact of AD on the atrophy patterns in subregions such as the hippocampus, amygdala, and thalamus, owing to their close neural correlation with memory and cognition, including episodic memory, emotional memory, executive function, and attention function [16–22]. They found that brain subregions in the

hippocampus, amygdala, and thalamus undergo atrophy in a manner that differs at varying stages of AD and that the predictive value of these atrophic changes for AD development varies as well [23–25]. Consequently, considering the heterogeneity of subregional structures in function and anatomy may lead to differential vulnerability to the AD spectrum, it is necessary to examine the changes in subregion volume at different stages of AD. The parietal lobe is known to be linked to episodic memory retrieval [26] and a deterioration in other parietal-associated cognitive performance, including spatial recognition and attentional processes is also observed in early AD [27,28]. A recent surface morphometry study revealed that the sulcus depth and cortical thickness of the parietal lobe were significantly altered in individuals diagnosed with AD and MCI [29]. Previous studies have analyzed the parietal lobe as a whole, thereby neglecting the pattern of atrophy in specific subregions of the parietal lobe [30,31]. This may be a contributing factor to the heterogeneity observed in the results of the studies [32,33].

The parietal lobe is a polymodal area, that has reported alterations in structural, metabolic, and functional characteristics in AD, predominantly in the posterior parietal cortex [34–37]. Functional magnetic resonance imaging (fMRI) study of the parietal lobes of patients with AD have emphasized its role in various cognitive functions, and the integrity of cognition-related brain connections [38]. Recent neuroimaging research elaborated on the importance of the "compensatory mechanism" in the temporoparietal junction, which is comprised of the angular and the supramarginal gyrus, on the relationship between the anosognosia with AD and default mode network [39]. Brain function changes in the inferior parietal lobule are reported in patients with MCI [40]. Notably, the parietal lobe could predict the development of AD. Hypometabolism of the left precuneus and posterior cingulate cortex may be a reliable marker for converting to AD [41]. Hypometabolism in other parietal areas, such as the parietal-temporal and inferior parietal lobe regions, was also a valid biomarker for distinguishing MCI at risk of developing AD dementia from stable MCI [42,43]. Chen *et al*. [44] demonstrated a significant reduction in grey matter volume in the superior parietal gyrus, inferior parietal gyrus, supramarginal gyrus, angular gyrus, and precuneus gyrus in individuals with progressive MCI (pMCI) compared to those with stable MCI (sMCI). Additionally, patients with progressive preclinical AD demonstrate atrophy of parietal structures [45]. However, the role of the volume of the parietal subregion in predicting the progression from CN to MCI and from MCI to AD remains unknown.

The Human Brainnetome Atlas (BNA-246), is a refined cross-validated atlas with more elaborate anatomical and functional connection modes for each area of the brain and contains 246 subregions in both hemispheres [46,47]. This study aimed to assess changes in the parietal subregion described by the BNA-246 in various stages of AD and identify the most predictive parietal subregion progression from MCI to AD and CN to MCI. We measured volume differences in subregions between LMCI and EMCI, CN and AD, LMCI and AD, CN and EMCI, pMCI and sMCI, and progressive CN (pCN) and stable CN (sCN). A receiver operating characteristic (ROC) curve was constructed to identify the best parietal subregion for differentiating between the AD, LMCI, EMCI, and CN groups. Additionally, the Cox proportional hazard models were applied to determine which specific parietal subregions, alone or in combination, could be used to predict progression from MCI to AD, and CN to MCI. Finally, we evaluated the correlation between cognition and the volume of the subregions in the four diagnostic groups. We hypothesize that certain subregions in the inferior parietal gyrus play an important role in differentiating between the different stages of AD and have a strong performance in predicting CN and MCI progression.

2. Materials and Methods

2.1 Database

The demographic and neuroimaging data used in the study were obtained from the Alzheimer's Disease Neuroimaging Initiative (ADNI) database (https://adni.loni.usc.edu). ADNI, launched in 2003, is an innovative public-private partnership, led by the Principal Investigator Michael W. Weiner, MD. Its original goal was to collate demographics, neuropsychological assessments, blood and CSF biological markers, genetic data, positron emission tomography (PET), and serial MRI to determine the development of MCI and early AD. Participants for the ADNI were recruited at various sites in Canada and the USA. More detailed information is accessible at https://adni.loni.usc.edu.

2.2 Participants and Classification Criteria

We recruited 662 individuals from the ADNI 2 and ADNI-GO. The participants selected for this study included individuals with CN (n = 228), EMCI (n = 221), LMCI (n = 112), and AD dementia (n = 101). All participants had completed neuropsychological assessments, including the Functional Activities Questionnaire (FAQ), Clinical Dementia Rating (CDR), Alzheimer's Disease Assessment Scale Cognitive (ADAS-cog 13), and the Mini-Mental State Examination (MMSE). T1-weighted MRI imaging was also available.

The participants were classified based on several cognitive scores, following the inclusion criteria provided by ADNI. CN participants had an MMSE score of 24–30 and a CDR score of 0 [23]. Individuals with MCI had subjective memory impairment reported by the patients, clinicians, or partners, an MMSE score of 24–30, a CDR score of 0, retained the function to maintain activities of daily living, and had no dementia. Individuals with MCI were further categorized as EMCI and LMCI based on their performance on the Wechsler Memory Scale's Logical Memory II subscale

Table 1. Subregions of the parietal lobe according to BNA-246.

Brain regions and subregions of the parietal lobe	Anatomical and modified Cyto-architectonic descriptions
SPL, Superior Parietal Lobule	
SPL_L(R)_5_1*	A7r, rostral area 7
SPL_L(R)_5_2	A7c, caudal area 7
SPL_L(R)_5_3	A5l, lateral area 5
SPL_L(R)_5_4	A7pc, postcentral area 7
SPL_L(R)_5_5	A7ip, intraparietal area 7 (hIP3)
IPL, Inferior Parietal Lobule	
IPL_L(R)_6_1	A39c, caudal area 39 (PGp)
IPL_L(R)_6_2	A39rd, rostrodorsal area 39 (Hip3)
IPL_L(R)_6_3	A40rd, rostrodorsal area 40 (PFt)
IPL_L(R)_6_4	A40c, caudal area 40 (PFm)
IPL_L(R)_6_5	A39rv, rostroventral area 39 (PGa)
IPL_L(R)_6_6	A40rv, rostroventral area 40 (PFop)
Pcun, Precuneus	
PCun_L(R)_4_1	A7m, medial area 7 (PEp)
PCun_L(R)_4_2	A5m, medial area 5 (PEm)
PCun_L(R)_4_3	dmPOS, dorsomedial parietooccipital sulcus (PEr)
PCun_L(R)_4_4	A31, area 31 (Lc1)
PoG, Postcentral Gyrus	
PoG_L(R)_4_1	A1/2/3ulhf, area 1/2/3 (upper limb, head and face region)
PoG_L(R)_4_2	A1/2/3tonIa, area 1/2/3 (tongue and larynx region)
PoG_L(R)_4_3	A2, area 2
PoG_L(R)_4_4	A1/2/3tru, area1/2/3 (trunk region)

* SPL_L(R)_5_1 and SPL_L_5_1 in left hemisphere or SPL_R_5_1 in right hemisphere. The other subregions have the same expression. BNA-246, the Human Brainnetome Atlas.

adjusted for years of education (including ImRec and DelRec) (EMCI: 9–11 for >16, 5–9 for >8–15, 3–6 for 0–7 years of education; LMC: <8 for >16, <4 for 8–15, <2 for 0–7 years of education). Apart from the National Institute of Neurological and Communicative Disorders and Stroke and the Alzheimer's Disease and Related Disorders Association (NINCDS/ADRDA) criteria, the MMSE scores of the patients with AD dementia was 20–26, with a CDR of 0.5 or 1.0. Individuals with schizophrenia, major depression, bipolar disorder, substance abuse, or a brain tumor; those who were unsuitable for MRI scanning; and those who have recently used psychoactive medication were excluded. Further details of inclusion and exclusion criteria are available at http://www.adni-info.org. The apolipoprotein E (APOE) ε4 allele is a high-risk gene for AD, individuals with one or more ε4 alleles were APOE ε4 carriers [48].

2.3 Neuroimaging Methods

The downloaded scans from ADNI were preprocessed with B1 non-uniformity correction, N3 bias field correction, and gradwarping corrections. The whole brain-based voxel-based morphometry (VBM) analysis was conducted using the computational anatomy toolbox (CAT12.8.2 (r2170) package, https://neuro-jena.github.io/cat/ [49]) and Statistical Parametric Mapping version 12 (SPM12, Wellcome Trust Center for Neuroimaging, London, UK; https://www.fil.ion.ucl.ac.uk/SPM) in MATLAB R2022b (MathWorks, Natick, MA, USA, [50]). First, the download images were input into SPM12 and manually repositioned to the standard AP/SI/LR orientations. Next, the 3D images were segmented into CSF, white matter, and gray matter (GM) in the CAT 12 package. Meanwhile, the total intracranial volume (TIV) was calculated. The GM images of all the participants were then spatially normalized into the 1.5-mm Montreal Neurological Institute space using the DARTEL algorithm, Finally, the GM images were scaled using Jacobian matrices and smoothed with a Gaussian kernel of $8 \times 8 \times 8$ full width at half maximum (FWHM).

The processed GM images served to extract subregional volumes. The parietal lobe was partitioned into four regions: superior parietal lobule (SPL), inferior parietal lobule (IPL), Precuneus (Pcun), and postcentral gyrus (PoG) as per the BNA-246 [47]. Furthermore, these regions were subdivided into several subregions; SPL, IPL, Pcun, and PoG were divided into 5, 6, 4, and 4 functional subregions, respectively. Therefore, in each hemisphere, the cortex of the parietal lobe was segmented into 19 subregions. Details about the subregions are provided inTable 1, ([46], reproduced with permission from [51]).

Table 2. Demographic and cognitive features of the individuals in four groups.

	CN (228)	EMCI (221)	LMCI (112)	AD (101)
Age	76 (11)	72 (10)	73 (11)	76 (11)
Sex (F/M)	117/111	89/132	57/55	40/61
Education (years)	16 (4)	16 (4)	16.5 (2)	16 (4)
MMSE	29 (2)	28 (3)	27 (4)	22 (5)
ADAS–cog 13	9 (5)	11 (8)	20 (11)	32 (13)
FAQ	0 (0)	11 (8)	20 (11)	15 (11)
CDR	0 (0)	0.5 (0)	0.5 (0)	1 (0.5)
APOE ε4 (Carries/no-carries)	65/163	90/131	68/44	66/35
Progressive/stable	52/176	32/189	53/59	

The continuous variables are presented as the median (interquartile range). Abbreviations: CN, cognitively normals; EMCI, early mild cognitive impairment; LMCI, late mild cognitive impairment; AD, Alzheimer's disease; F, Female; M, Male; APOE, apolipoprotein E gene; MMSE, Mini-Mental State Examination; ADAS–cog, Alzheimer's Disease Assessment Scale–Cognitive Subscale; FAQ, Functional Activities Questionnaire; CDR, Clinical Dementia Rating.

Table 3. Demographic features of the individuals in progressive and stable group in CN and MCI.

	pCN (52)	sCN (176)	pMCI (85)	sMCI (248)
Age	79 (8)	75.5 (10)	74 (10)	71.5 (11)
Sex (F/M)	26/26	91/85	37/48	109/139
Education (years)	16 (4)	16 (4)	16 (4)	16 (4)
Follow-up (years)	6.3 ± 3.4	7 ± 4	3.2 ± 2.5	5 ± 3.2

The continuous variables are presented as the median (interquartile range) or mean $\pm$ standard deviation. Abbreviations: pCN, progressive cognitively normals; sCN, stable cognitively normals; pMCI, progressive mild cognitive impairment; sMCI, stable mild cognitive impairment; F, Female; M, Male.

2.4 Statistical Analysis

Statistical analyses were conducted using the IBM SPSS (Statistical Product and Service Solutions) Statistics software version 25 (IBM Corp, Armonk, NY, USA, [52]). All the continuous variables are summarized as the median (interquartile range). The distributions of sex and APOE ε4 carriers and non-carrier composition were assessed by chi-squared test. The continuous variables were analyzed by the nonparametric Kruskal–Wallis test. Mann–Whitney U tests were used to compare continuous variables between pCN and sCN groups as well as pMCI and sMCI groups. Analysis of covariance (ANCOVA) was carried out with education level, sex, TIV, APOE, and age as covariates to compare the gray matter volume differences in parietal subregions between AD/CN, EMCI/CN, LMCI/EMCI, and AD/LMCI to model the trajectory of parietal lobe atrophy. The APOE variable was included as a covariate because it has been reported that the presence of APOE ε4 alters the pattern of GM changes in AD [48]. ANCOVA was also used to compare subregion volumes between pCN and sCN groups and pMCI and sMCI groups. The Bonferroni correction was applied to all multiple comparisons and the comparisons of pCN and sCN groups as well as pMCI and sMCI. Furthermore, the area under the curve (AUC) of the ROC curve was calculated as an indicator of the ability of the subregions to differentiate between AD, LMCI, EMCI, and CN groups. In addition, the Cox proportional hazards regression analysis was performed to evaluate the associations between parietal subregion atrophy and predict progression from MCI to AD and CN to MCI. The independent variable for each analysis was the volume of one of the parietal subregions. Hazard ratio (HR) values for each subregion were interpreted as an increased risk of progression from MCI to AD and from CN to MCI for each standard deviation reduction in parietal subregion volume. Model 1 shows the unadjusted HR for the CN and MCI groups; model 2 shows HR adjusted for age, sex, TIV, and education in the CN and MCI groups. Next, to evaluate the combined predictive value of the best combination of markers, we performed a forward stepwise Cox regression analysis with all baseline parietal subregion volumes as possible predictors in both CN and MCI groups. Finally, we applied partial correlation analysis to evaluate the associations between subregion volume and neuropsychological assessment (MMSE, ADAS-cog 13, FAQ) across different groups, with education level, TIV, APOE, age, and sex as covariates. The significance level was set at $p < 0.05$ and the tests were two-sided in all analyses.

Table 4. Comparison of the volume of parietal subregions among the four groups.

		CN-EMCI		EMCI-LMCI		LMCI-AD		CN-AD	
	p	average value difference	*p*	average value difference	*p*	average value difference	*p*	average value difference	*p*
SPL	0.000**	–0.183	0.653	0.343	0.085	0.382	0.156	0.542	0.002*
SPL_L_5_1	0.024*	–0.030	0.297	0.034	0.425	0.023	1	0.027	1.000
SPL_R_5_1	0.010*	–0.006	1	0.039	0.998	0.055	0.653	0.088	0.022*
SPL_L_5_2	0.024*	–0.008	1	0.034	0.617	0.029	1	0.054	0.086
SPL_R_5_2	0.007*	–0.023	1	0.031	0.962	0.050	0.367	0.058	0.086
SPL_L_5_3	0.010*	–0.013	1	0.040	0.309	0.029	1	0.057	0.071
SPL_R_5_3	0.001*	–0.018	1	0.033	0.267	0.038	0.376	0.053	0.019*
SPL_L_5_4	0.038*	–0.032	0.347	0.032	0.705	0.027	1	0.028	1
SPL_R_5_4	0.011*	–0.028	0.665	0.025	1	0.053	0.304	0.049	0.225
SPL_L_5_5	0.057	–0.003	1	0.021	1	0.026	1	0.045	0.119
SPL_R_5_5	0.001*	–0.021	1	0.053	0.197	0.051	0.553	0.083	0.011*
IPL	0.000**	0.385	1	1.215	0.022*	2.287	0.000**	3.887	0.000**
IPL_L_6_1	0.000**	0.027	1	0.142	0.039*	0.133	0.223	0.302	0.000**
IPL_R_6_1	0.000**	0.036	1	0.073	1	0.308	0.000**	0.417	0.000**
IPL_L_6_2	0.000**	–0.017	1	0.058	0.762	0.107	0.130	0.148	0.002*
IPL_R_6_2	0.000**	0.021	1	0.046	1	0.119	0.099	0.186	0.000**
IPL_L_6_3	0.000**	0.015	1	0.107	0.084	0.142	0.045*	0.264	0.000**
IPL_R_6_3	0.000**	0.008	1	0.058	1	0.221	0.001*	0.286	0.000**
IPL_L_6_4	0.000**	0.049	1	0.158	0.004*	0.097	0.508	0.305	0.000**
IPL_R_6_4	0.000**	0.060	1	0.152	0.041*	0.202	0.021*	0.414	0.000**
IPL_L_6_5	0.000**	0.061	1	0.212	0.012*	0.327	0.001*	0.600	0.000**
IPL_R_6_5	0.000**	0.078	0.493	0.073	1	0.313	0.000**	0.465	0.000**
IPL_L_6_6	0.000**	–0.020	1	0.113	0.235	0.184	0.037*	0.278	0.000**
IPL_R_6_6	0.011*	0.067	1	0.022	1	0.134	0.487	0.223	0.006*

Table 4. Continued.

		CN-EMCI		EMCI-LMCI		LMCI-AD		CN-AD	
	p	average value difference	*p*	average value difference	*p*	average value difference	*p*	average value difference	*p*
Pcun	0.000**	–0.443	0.095	0.466	0.231	1.050	0.001*	1.073	0.000**
PCun_L_4_1	0.000**	–0.063	0.071	0.058	0.369	0.082	0.182	0.076	0.133
PCun_R_4_1	0.001*	–0.034	0.574	0.036	0.946	0.072	0.118	0.074	0.042*
PCun_L_4_2	0.112	–0.039	0.551	0.035	1	0.033	1	0.029	1
PCun_R_4_2	0.000**	–0.034	0.955	0.045	0.737	0.097	0.044*	0.108	0.004*
PCun_L_4_3	0.001*	–0.068	0.452	0.039	1	0.168	0.023*	0.139	0.039*
PCun_R_4_3	0.000**	–0.114	0.081	0.067	1	0.207	0.016*	0.161	0.051
PCun_L_4_4	0.000**	–0.034	1	0.115	0.050	0.146	0.037*	0.227	0.000**
PCun_R_4_4	0.000**	–0.057	1	0.071	1	0.245	0.001*	0.259	0.000**
PoG	0.010	–0.386	0.039*	0.230	1	0.303	0.931	0.146	1
PoG_L_4_1	0.161	–0.065	0.210	0.035	1	0.028	1	–0.002	1
PoG_R_4_1	0.077	–0.077	0.076	0.023	1	0.036	1	–0.017	1
PoG_L_4_2	0.012*	–0.016	1	0.092	0.024*	–0.020	1	0.056	0.626
PoG_R_4_2	0.340	–0.029	1	0.022	1	0.037	1	0.030	1
PoG_L_4_3	0.009*	–0.035	0.950	0.040	1	0.072	0.334	0.077	0.124
PoG_R_4_3	0.028*	–0.041	1	0.006	1	0.109	0.105	0.074	0.402
PoG_L_4_4	0.030*	–0.063	0.023*	0.013	1	0.020	1	–0.030	1
PoG_R_4_4	0.003*	–0.060	0.004*	–0.001	1	0.020	1	–0.041	0.482

*$p < 0.05$, **$p < 0.001$. The *p*-values are Bonferroni corrected values.

3. Results

3.1 Characteristics of Individuals

All the demographics and cognitive features of the individuals are shown in Table 2. The level of education (H = 6.36, $p = 0.095$) did not differ significantly between all groups. The sex composition of the four groups differed significantly ($X^2 = 8.248$, $p = 0.041$). However, none of the observed differences were statistically significant after correcting for multiple comparisons using the Bonferroni method. The distribution of APOE ε4 non-carriers and carriers differed significantly between all groups ($X^2 = 54.607$, $p < 0.001$), except LMCI and AD. Age differences were observed between individuals with EMCI and AD, EMCI and CN, and LMCI and CN (H = 42.049, $p < 0.001$). For all groups except those diagnosed with LMCI and EMCI, a significant difference in CDR score was found between individuals in all groups (H = 497.298, $p < 0.001$). All groups showed significant differences in the ADAS-cog 13, FAQ, and MMSE scores (H = 305.253, $p < 0.001$, H = 346.871, $p < 0.001$, and H = 280.472, $p < 0.001$, respectively).

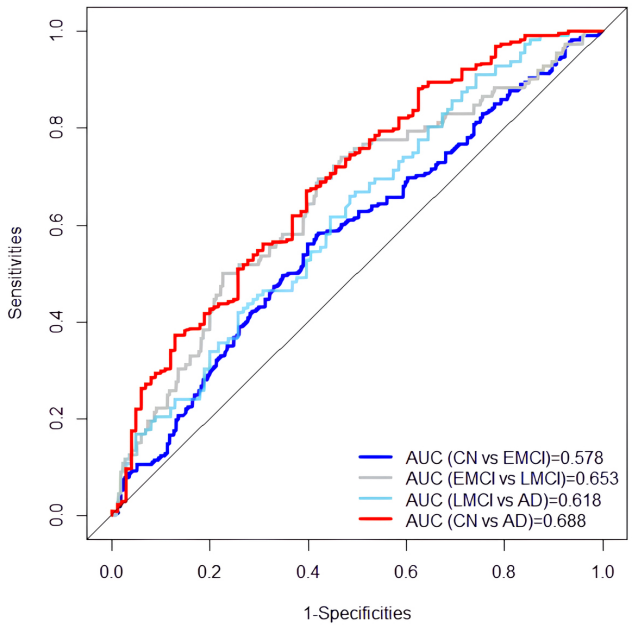

Fig. 1. The ROC curve of left IPL_6_5 volume in differentiating between CN and EMCI (blue), EMCI and LMCI (gray), LMCI and AD (cyan), and CN and AD (red). AUC, area under the curve; ROC, receiver operating characteristic; AD, Alzheimer's disease; EMCI, early mild cognitive impairment; LMCI, late early mild cognitive impairment; CN, cognitively normal; IPL, inferior parietal lobule; IPL_6_5, left rostroventral area 39 in inferior parietal lobule.

A total of 52 individuals with CN at baseline progressed to MCI within approximately six years, while 85 patients with MCI at baseline progressed to AD within approximately three years (Table 3). There was no significant difference in sex distribution and education level between the sCN and pCN groups ($X^2 = 0.047$, $p = 0.829$; Z = 1.517, $p = 0.129$), as well as the sMCI and pMCI groups ($X^2 = 0.005$, $p = 0.946$; Z = –0.64, $p = 0.522$). However, the age was significantly higher in the pCN group than the sCN group (Z = –3.352, $p = 0.001$). Similarly, the age was significantly higher in the pMCI group than the sMCI group (Z = –2.186, $p = 0.029$).

3.2 Neuroimaging of Region Volume

The comparison of volumes in parietal regions and subregions among the four diagnosed groups is shown in Table 4. All p-values indicate the results after correction using the Bonferroni method. Significant differences in volumes of the Pcun, IPL, PoG and SPL were observed between the four groups, as indicated by the ANCOVA results (all $p < 0.05$). Further pairwise comparisons revealed that the EMCI group had a significant increase in the volume of the PoG ($p = 0.038$) compared to the CN group. The LMCI group exhibited significantly reduced volumes of the IPL ($p = 0.022$) compared to the EMCI group. The AD group showed significant volume reductions in the IPL ($p < 0.001$) and Pcun ($p = 0.001$) compared to the LMCI group. Comparing the CN and AD groups, patients with AD exhibited more widespread significant volume loss in the SPL ($p = 0.002$), IPL ($p < 0.001$), and Pcun ($p < 0.001$) compared to those with CN. The volumes of the parietal regions and subregions are displayed in **Supplementary Table 1**.

When comparing the volume of different parietal subregions, individuals with EMCI showed a significant increase in volume in two subregions compared to individuals with CN. On the other hand, individuals with LMCI exhibited significantly reduced volumes in five subregions compared to the EMCI group. Furthermore, individuals with AD showed significant volume reductions in twelve subregions compared to those with LMCI. When compared to individuals with CN, those with AD showed significant volume loss in twenty subregions.

Table 5 provides a comparison of the volume of parietal subregions between individuals with pCN and sCN as well as those with pMCI and sMCI. The pCN group exhibited significantly reduced volumes in the SPL ($p = 0.032$), IPL ($p = 0.007$), and POG ($p = 0.012$), as well as seven subregions, compared to the sCN group. Similarly, the pMCI groups showed a significant reduction in volume in the SPL ($p = 0.016$), IPL ($p = 0.01$), Pcun ($p = 0.036$), and nine subregions compared to sMCI group. Detailed information regarding the parietal region and subregion volumes for progressive and stable individuals of CN and MCI can be found in **Supplementary Table 2.**

3.3 Subregional Differentiation and Prediction Ability

Table 6 provides the AUC values for the four comparison groups. In all the subregions, the left IPL_6_5 (rostro-

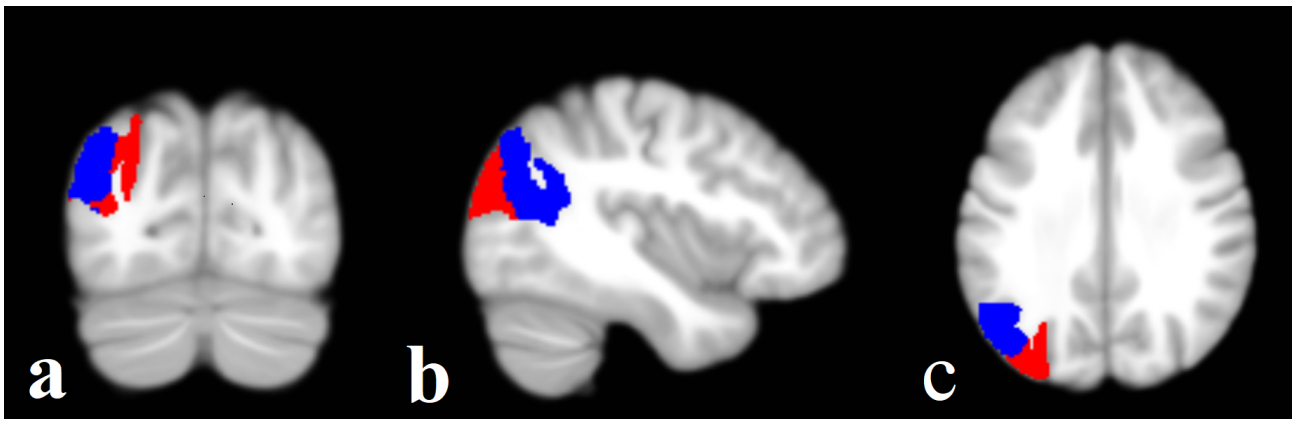

Fig. 2. The anatomical location of left IPL_6_5 (blue) and left IPL_6_1 (red) in the parietal lobe. (a) Coronal. (b) Sagittal. (c) Axial. IPL_6_5, rostroventral area 39 in inferior parietal lobule. IPL_6_1, caudal area 39 in inferior parietal lobule.

ventral area 39) exhibited the best discrimination between AD and CN, with an AUC of 0.688 (Fig. 1). The anatomical location of the left IPL_6_5 is shown in Fig. 2.

Cox proportional hazards regression analysis results showed, in the model of CN, a smaller volume of right SPL_5_2, SPL_5_4, and bilateral IPL_6_5 conferred a higher risk of progression from CN to MCI (Table 7) (all $p < 0.05$). On adjustment for age, sex, TIV, and education, bilateral IPL_6_5 remained significant (Table 8) (both $p < 0.05$). In the model of MCI, many subregions could significantly predict MCI conversion risk even after age, sex, TIV, and education correction (Tables 9,10). When using a forward stepwise model to select the best predictors, the left IPL_6_4 and bilateral IPL_6_5 are statistically significant in the CN model (all $p < 0.05$) (Table 11) while only the left IPL_6_1 remained statistically significant in the MCI model ($p < 0.001$) (Table 12). The anatomical location of left IPL_6_1 is depicted in Fig. 2.

3.4 Correlation of Subregion Volume with Cognitive Score

Supplementary Tables 3,4,5 show the results of the correlation analysis of subregion volume and MMSE, FAQ, and ADAS-cog 13 score. A mild correlation was found between the MMSE score and four subregions in patients with EMCI, two subregions in patients with LMCI, and the three subregions in patients with AD (all $p < 0.001$). Furthermore, a robust correlation was found between the ADAS-cog 13 score and the three subregions in patients with LMCI, and six subregions in patients with AD (all $p < 0.001$). Additionally, the right IPL_6_2 exhibited a significant correlation with FAQ in LMCI ($p < 0.05$).

4. Discussion and Limitations

4.1 Discussion

This study employed voxel-based morphometry to investigate the atrophy trajectory of the parietal subregions across the AD continuum and to identify parietal subregions with significant predictive capacity for conversion from MCI to AD or from CN to MCI. The findings are summarized as follows.

(1) Areas of abnormal parietal volume spread widely with the further cognitive decline. Abnormalities in the volume of the PoG have been observed in early MCI, followed by declines in the volumes of the IPL, Pcun, and SPL.

(2) Subregion differentiation ability analysis revealed that the left IPL_6_5 is the best subregion to discriminate AD from CN (AUC = 0.688). Cox proportional hazards regression analysis revealed that the baseline bilateral IPL_6_5 volume predicted progression from CN to MCI during approximately six years of clinical follow-up. When including all baseline volumes as candidate predictors, forward stepwise Cox regression revealed that the combined predictive value of baseline the left IPL_6_4 and bilateral IPL_6_5 volume exhibits statistical significance in the CN model, meanwhile, only the left IPL_6_1 exhibits a significant predictive value in the MCI model.

(3) Correlation analysis showed a robust association between ADAS-Cog 13 and MMSE scores and most IPL and SPL subregions in individuals with MCI and AD. The FAQ score showed a significant correlation with the right IPL_6_2 in LMCI individuals.

The parietal lobe plays a crucial role in various higher cognitive processes and has extensive connections with other brain regions, such as the thalamus, prefrontal cortex, cingulate cortex, and (para)hippocampus [37,53,54], making it susceptible to degenerative lesions [55]. As previous studies have focused on subregions of the frontal lobe, hippocampus, and amygdala [15,51], this research specifically investigates atrophy in the parietal subregion to gain a further understanding of the neuroimaging mechanisms underlying AD. The volume of the PoG was found to significantly increase in the early MCI group compared to the CN group. This could be a macroscopic manifestation of early compensatory mechanisms to counter impending brain damage [56,57]. Neuroinflammation may also play a role, as evidence suggests that it peaks in the earliest stages of AD

Table 5. Comparison of the volume of parietal subregions between pCN and sCN as well as pMCI and sMCI groups.

	sCN-pCN		sMCI-pMCI	
	average value difference	*p*	average value difference	*p*
SPL	0.366	0.032*	0.377	0.016*
SPL_L_5_1	0.028	0.261	0.034	0.122
SPL_R_5_1	0.009	0.803	0.007	0.821
SPL_L_5_2	0.055	0.031*	0.066	0.003*
SPL_R_5_2	0.075	0.007*	0.046	0.055
SPL_L_5_3	0.032	0.234	0.048	0.040*
SPL_R_5_3	0.028	0.186	0.027	0.173
SPL_L_5_4	0.042	0.112	0.046	0.057
SPL_R_5_4	0.046	0.101	0.017	0.504
SPL_L_5_5	0.030	0.194	0.028	0.157
SPL_R_5_5	0.021	0.552	0.057	0.032*
IPL	1.350	0.007*	1.237	0.010*
IPL_L_6_1	0.086	0.208	0.156	0.007*
IPL_R_6_1	0.137	0.069	0.062	0.362
IPL_L_6_2	0.028	0.551	0.071	0.101
IPL_R_6_2	0.100	0.068	0.124	0.004*
IPL_L_6_3	0.092	0.092	0.082	0.104
IPL_R_6_3	0.087	0.151	0.125	0.019*
IPL_L_6_4	0.010	0.856	0.120	0.024*
IPL_R_6_4	0.066	0.355	0.177	0.006*
IPL_L_6_5	0.304	0.001*	0.148	0.060
IPL_R_6_5	0.227	0.001*	0.112	0.074
IPL_L_6_6	0.101	0.165	0.075	0.240
IPL_R_6_6	0.113	0.171	0.014	0.840
Pcun	0.456	0.112	0.517	0.036*
PCun_L_4_1	0.023	0.561	0.059	0.091
PCun_R_4_1	0.035	0.299	0.031	0.266
PCun_L_4_2	0.049	0.172	0.046	0.154
PCun_R_4_2	0.049	0.203	0.046	0.166
PCun_L_4_3	0.069	0.280	0.058	0.265
PCun_R_4_3	0.118	0.129	0.118	0.056
PCun_L_4_4	–0.014	0.806	0.093	0.048*
PCun_R_4_4	0.098	0.171	0.065	0.231
POG	0.572	0.012*	0.052	0.789
PoG_L_4_1	0.069	0.159	–0.002	0.958
PoG_R_4_1	0.066	0.191	0.006	0.882
PoG_L_4_2	0.097	0.025*	–0.024	0.501
PoG_R_4_2	0.113	0.010*	–0.016	0.641
PoG_L_4_3	0.070	0.104	0.037	0.272
PoG_R_4_3	0.114	0.018*	0.038	0.381
PoG_L_4_4	0.012	0.723	0.010	0.750
PoG_R_4_4	0.031	0.307	0.004	0.869

Abbreviations: pCN, progressive cognitively normals; sCN, stable cognitively normals; pMCI, progressive mild cognitive impairment; sMCI, stable mild cognitive impairment. *$p < 0.05$. The *p*-values are Bonferroni corrected values.

[58], and neuroinflammation has been observed in the inferior parietal cortex in early AD [59]. The Pcun and IPL shrink with cognitive decline, these results align with previous research that has noted volume loss in the Pcun and IPL during the early prodromal stages of AD [60].

The BNA-246 partitioned Brodmann Area 39 (BA 39) into three areas: caudal (IPL_6_1), rostrodorsal (IPL_6_2), and rostroventral (IPL_6_5). Similarly, BA 40 was partitioned into rostrodorsal (IPL_6_3), caudal (IPL_6_4), and rostroventral (IPL_6_6) areas. BA 39 corresponds to the angular gyrus (AG). Specifically, the caudal (IPL_6_1) and rostroventral (IPL_6_5) areas represent two major subregions of the AG with distinct cytoarchitectures, PGp and PGa, respectively. In our study, the left IPL_6_5 performed best in the distinction between CN and AD and could best differentiate between EMCI and LMCI (although the AUC was not high). This suggests that the left IPL_6_5 may play an important role in AD development. This conclusion is further supported by forward stepwise Cox regression, which revealed that the baseline volume change in the

Table 6. The ability of parietal subregion volume to differentiate between the four diagnostic groups.

Subregion	EMCI VS CN		EMCI VS LMCI		LMCI VS AD		AD VS CN	
	AUC	*p*	AUC	*p*	AUC	*p*	AUC	*p*
SPL_L_5_1	0.604	0.000**	0.592	0.006*	0.543	0.280	0.540	0.251
SPL_R_5_1	0.570	0.011*	0.563	0.060	0.589	0.025*	0.590	0.009*
SPL_L_5_2	0.586	0.002*	0.589	0.008*	0.540	0.314	0.547	0.177
SPL_R_5_2	0.602	0.000**	0.586	0.010*	0.543	0.273	0.533	0.342
SPL_L_5_3	0.580	0.004*	0.585	0.011*	0.574	0.062	0.575	0.029*
SPL_R_5_3	0.628	0.000**	0.594	0.005*	0.602	0.010*	0.586	0.013*
SPL_L_5_4	0.614	0.000**	0.579	0.018*	0.572	0.068	0.539	0.254
SPL_R_5_4	0.618	0.000**	0.570	0.037*	0.596	0.015*	0.562	0.075
SPL_L_5_5	0.556	0.041*	0.568	0.043*	0.569	0.083	0.580	0.021*
SPL_R_5_5	0.613	0.000**	0.613	0.001*	0.600	0.012*	0.586	0.013*
IPL_L_6_1	0.582	0.003*	0.642	0.000**	0.542	0.294	0.600	0.004*
IPL_R_6_1	0.580	0.003*	0.577	0.021*	0.632	0.001*	0.628	0.000**
IPL_L_6_2	0.582	0.003*	0.572	0.031*	0.586	0.030*	0.585	0.014*
IPL_R_6_2	0.562	0.023*	0.571	0.035*	0.589	0.024*	0.604	0.003*
IPL_L_6_3	0.588	0.001*	0.617	0.000**	0.597	0.015*	0.637	0.000**
IPL_R_6_3	0.595	0.000**	0.583	0.013*	0.634	0.001*	0.636	0.000**
IPL_L_6_4	0.560	0.028*	0.638	0.000**	0.567	0.092	0.644	0.000**
IPL_R_6_4	0.551	0.064	0.618	0.000**	0.590	0.023*	0.651	0.000**
IPL_L_6_5	0.578	0.004*	0.653	0.000**	0.618	0.003*	0.688	0.000**
IPL_R_6_5	0.559	0.030*	0.585	0.011*	0.628	0.001*	0.659	0.000**
IPL_L_6_6	0.606	0.000**	0.596	0.004*	0.626	0.002*	0.620	0.001*
IPL_R_6_6	0.588	0.001*	0.547	0.157	0.635	0.001*	0.564	0.063
PCun_L_4_1	0.630	0.000**	0.599	0.003*	0.564	0.107	0.551	0.139
PCun_R_4_1	0.600	0.000**	0.572	0.032*	0.581	0.042*	0.557	0.096
PCun_L_4_2	0.606	0.000**	0.565	0.051	0.556	0.160	0.516	0.647
PCun_R_4_2	0.619	0.000**	0.593	0.006*	0.594	0.018*	0.577	0.026*
PCun_L_4_3	0.642	0.000**	0.566	0.051	0.593	0.019*	0.526	0.458
PCun_R_4_3	0.652	0.000**	0.586	0.011*	0.608	0.006*	0.540	0.251
PCun_L_4_4	0.623	0.000**	0.630	0.000**	0.569	0.082	0.573	0.034*
PCun_R_4_4	0.628	0.000**	0.604	0.002*	0.611	0.005*	0.591	0.009*
PoG_L_4_1	0.662	0.000**	0.564	0.057	0.561	0.127	0.467	0.342
PoG_R_4_1	0.663	0.000**	0.548	0.149	0.579	0.046*	0.465	0.312
PoG_L_4_2	0.606	0.000**	0.599	0.003*	0.521	0.595	0.509	0.786
PoG_R_4_2	0.609	0.000**	0.551	0.126	0.558	0.143	0.503	0.923
PoG_L_4_3	0.634	0.000**	0.590	0.007*	0.591	0.022*	0.546	0.184
PoG_R_4_3	0.616	0.000**	0.545	0.177	0.624	0.002*	0.563	0.070
PoG_L_4_4	0.664	0.000**	0.565	0.051	0.568	0.086	0.462	0.272
PoG_R_4_4	0.671	0.000**	0.560	0.074	0.541	0.306	0.429	0.040*

*$p < 0.05$, **$p < 0.001$.

Table 7. HRs and 95% CIs for progression to MCI within CN groups.

Subregion	*p*-value	HRs (95.0% CI)
SPL_R_5_2	0.044	0.219 (0.050 to 0.959)
SPL_R_5_4	0.046	0.163 (0.027 to 0.968)
IPL_L_6_5	0.031	0.610 (0.390 to 0.955)
IPL_R_6_5	0.036	0.565 (0.332 to 0.962)

Model 1 of the CN. Abbreviation: HR, hazard ratio.

left IPL_6_4 combined with bilateral IPL_6_5 could predict CN progression to MCI. Researchers have examined the parietal lobe as a whole in previous studies of AD's diagnosis and prediction [30,55]. The posterior cingulate, the precuneus, the inferior parietal lobe, and the posterior parietal lobe, composition of the parietotemporal cortex, serve as reliable imaging biomarkers for discriminating between pMCI and sMCI in both sMRI and metabolic studies [42–44,61]. However, it should be noted that these non-specific areas encompass various regions, including the AG, supramarginal gyrus (SMG), and BA 31 [62]. This could explain

Table 8. HRs and 95% CIs for progression to AD within MCI groups.

Subregion	*p*-value	HRs (95.0% CI)
SPL_L_5_2	<0.001	0.094 (0.029 to 0.301)
SPL_R_5_2	0.003	0.188 (0.061 to 0.573)
SPL_L_5_3	0.002	0.124 (0.033 to 0.466)
SPL_R_5_3	0.023	0.193 (0.047 to 0.797)
SPL_L_5_4	0.019	0.272 (0.092 to 0.805)
SPL_L_5_5	0.009	0.133 (0.029 to 0.606)
SPL_R_5_5	0.002	0.191 (0.066 to 0.556)
IPL_L_6_1	<0.001	0.365 (0.229 to 0.583)
IPL_R_6_1	0.018	0.647 (0.450 to 0.929)
IPL_L_6_2	0.001	0.322 (0.165 to 0.626)
IPL_R_6_2	<0.001	0.288 (0.155 to 0.536)
IPL_L_6_3	0.007	0.475 (0.276 to 0.818)
IPL_R_6_3	0.001	0.423 (0.254 to 0.704)
IPL_L_6_4	<0.001	0.389 (0.232 to 0.650)
IPL_R_6_4	<0.001	0.476 (0.315 to 0.719)
IPL_L_6_5	<0.001	0.514 (0.367 to 0.721)
IPL_R_6_5	0.001	0.506 (0.339 to 0.755)
IPL_L_6_6	0.021	0.625 (0.419 to 0.931)
PCun_L_4_1	0.016	0.407 (0.196 to 0.846)
PCun_R_4_3	0.004	0.539 (0.353 to 0.825)
PCun_L_4_4	0.003	0.465 (0.282 to 0.768)
PCun_R_4_4	0.010	0.561 (0.362 to 0.869)
PoG_L_4_3	0.041	0.423 (0.185 to 0.966)

Model 1 of the MCI. Abbreviation: HR, hazard ratio.

Table 9. Adjusted HRs and 95% CIs for progression to MCI within CN groups.

Subregion	*p*-value	HRs (95.0% CI)
IPL_L_6_5	0.016	0.465 (0.249 to 0.868)
IPL_R_6_5	0.030	0.430 (0.200 to 0.922)

Model 2 of the CN adjusted for age, sex, TIV, and level of education. Abbreviation: HR, hazard ratio; TIV, total intracranial volume.

Table 10. Adjusted HRs and 95% CIs for progression to AD within MCI groups.

Subregion	*p*-value	HRs (95.0% CI)
SPL_L_5_2	<0.001	0.040 (0.010 to 0.166)
SPL_R_5_2	0.002	0.131 (0.036 to 0.473)
SPL_L_5_3	0.008	0.147 (0.036 to 0.607)
SPL_L_5_4	0.038	0.260 (0.073 to 0.928)
SPL_L_5_5	0.011	0.114 (0.022 to 0.604)
SPL_R_5_5	0.005	0.196 (0.062 to 0.617)
IPL_L_6_1	<0.001	0.313 (0.180 to 0.546)
IPL_R_6_1	0.042	0.644 (0.421 to 0.984)
IPL_L_6_2	0.001	0.284 (0.136 to 0.593)
IPL_R_6_2	<0.001	0.195 (0.093 to 0.410)
IPL_L_6_3	0.042	0.532 (0.289 to 0.978)
IPL_R_6_3	0.006	0.443 (0.248 to 0.790)
IPL_L_6_4	0.001	0.357 (0.199 to 0.641)
IPL_R_6_4	<0.001	0.420 (0.263 to 0.670)
IPL_L_6_5	<0.001	0.496 (0.336 to 0.732)
IPL_R_6_5	0.001	0.446 (0.276 to 0.718)
PCun_L_4_1	0.014	0.359 (0.158 to 0.813)
PCun_R_4_3	0.011	0.521 (0.315 to 0.862)
PCun_L_4_4	0.003	0.379 (0.198 to 0.723)
PCun_R_4_4	0.022	0.529 (0.306 to 0.912)

Model 2 of the MCI adjusted for age, sex, TIV, and level of education. Abbreviation: HR, hazard ratio.

Table 11. The combined subregion of HRs and 95% CIs for progression to MCI within CN groups.

Subregion	*p*-value	HRs (95.0% CI)
IPL_L_6_4	0.001	5.671 (1.993 to 16.135)
IPL_L_6_5	0.043	0.524 (0.280 to 0.979)
IPL_R_6_5	0.018	0.342 (0.140 to 0.835)

Abbreviation: HR, hazard ratio.

Table 12. The combined subregion of HRs and 95% CIs for progression to AD within MCI groups.

Subregion	*p*-value	HRs (95.0% CI)
IPL_L_6_1	<0.001	0.365 (0.229 to 0.583)

Abbreviation: HR, hazard ratio.

why the AG has not been emphasized in previous structural articles focusing on MCI discrimination. Our study provides further evidence that PGa of the AG may play a specific role in the onset of AD. This result indicated the importance of monitoring neuropathological changes in this structure during the pre-AD period to prevent further cognitive decline. BA40 corresponds to the SMG, and its involvement in the development of AD has been reported [63], but the present study is the first to report the association of caudal BA40 in CN conversion. Additionally, the volume change of the left IPL_6_1 is best in predicting the development of MCI into AD for approximately three years. Thus, on the other hand, PGp of the AG plays a key role in the evolution of MCI to AD. This result is consistent with those of previous study which reported that the left AG shows potential as a marker for monitoring the progression of amnestic MCI (aMCI) and cognitive decline [64].

AG is a higher-order associative cortical area engaged in the integration of multiple sensory systems [62], and it is anatomically and functionally connected to many regions of the brain [65]. Functional study has found significant reductions in AG connectivity to a wide range of brain regions such as the parietal, frontal, temporal, and occipital cortex in the pMCI group compared with the sMCI group [66]. Abnormal tau deposition in the middle frontal cortex, superior temporal cortex, and AG have been found in autopsies

of individuals with AD [67]. Therefore, we hypothesize that there may be a widespread disruption of AG connectivity with other brain regions or abnormal protein deposition leading to structural atrophy of the AG, a change that plays a role in the onset and development of AD. PGp and PGa of the AG can be characterized by specific functional and connectivity patterns. The PGp demonstrates greater functional connectivity and fiber density with the (para)hippocampus and precuneus compared to PGa [62]. The closer anatomical and functional connectivity of the GpG with early AD-involved regions may explain why the left IPL_6_1 is more relevant in predicting the progression of MCI to AD. Another study found significant atrophy of the left hippocampus, temporal pole, and angular gyrus in AD compared with behavioral variant frontotemporal dementia [68]. Further studies are needed for the specificity of the angular gyrus subregion in AD. The PGp is primarily involved in visual perception, while the PGa is more associated with integrating multisensory information [55]. Additionally, the AG is involved in word recognition, episodic and semantic retrieval, and mathematical cognition [69,70].

In populations that age normally, hemispheric specialization is thought to contribute to the speed of processing information [71]. Brain atrophy in AD is bilateral, but may not be hemispherically symmetrical. Grey matter loss occurs earlier and more severely in the left hemisphere in AD [72]. It is reported that a wide range of brain structures, such as the hippocampus, amygdala, and caudate show asymmetric atrophy in AD and MCI [73–75]. The left side IPL_6_5 was more significantly atrophied than the right side when comparing AD and CN with EMCI and LMCI in our study. Although both sides significantly predicted the progression of CN to MCI, the left side had a greater HR than the right. Therefore, the angular gyrus shows asymmetry in the distinction between different stages of AD and in the predictive value of CN and MCI, with the left side being more significant. Amyloid deposition in the angular gyrus was asymmetric and associated with hypometabolism [76]. Another study reported asymmetric tau protein deposition in AD [77]. Thus, asymmetric atrophy of the angular gyrus may arise from asymmetric pathological changes. Therefore, it is necessary to investigate the correlation between the asymmetry of grey matter atrophy in the subregion of the AG and protein deposition in the fortune. In our study, significant differences in IPL and Pcun volumes were observed between the EMCI and LMCI groups, as well as between the LMCI and AD groups. Correlations were also found between certain subregional volumes of the IPL and SPL and scores on the ADAS-Cog 13, FAQ, and MMSE scales in AD and MCI. The parietal lobe's role as a sensory and motor region, with its connections to other brain regions, may explain these correlations with cognitive scales [53].

4.2 Limitations

Although we have analyzed the subregions, providing a more detailed atrophy trajectory and subregional prediction of parietal in the AD continuum, the current study had certain limitations. First, this was a baseline state cross-sectional study, to confirm the results of this study, future longitudinal studies are necessary to comprehensively investigate the full course of parietal lobe atrophy. Second, due to the variability of different atlas, the use of other templates is necessary to validate the results of this study. Third, although structural studies can quantify brain volume, parietal hypometabolism is an important feature in AD. Future studies should combine structural (white matter, gray matter), functional connectivity, and metabolic information to reveal subregional pathological changes in the parietal lobes. Fourth, of all the parietal subregions, the left IPL_6_5 had the highest AUC value for discriminating between AD and CN (AUC value = 0.688), but this was only moderately discriminant. Fifth, although VBM can quantify the volume of grey matter, there is some error due to space standardization and matching of templates, etc., so a more accurate software, FreeSufer [78], should be used to validate the findings in this study. Finally, the recruitment of participants from different locations and ethnicities will be important for the replication of this experiment and the confirmation of its findings.

5. Conclusion

Among all the parietal subregions, the left IPL_6_5 exhibited the best effectiveness in differentiating between AD and CN. The Cox model consisting of the left IPL_6_4 and bilateral IPL_6_5 was most effective in predicting CN progression to MCI. Additionally, the left IPL_6_1 showed the best predictive power in predicting the progression of MCI to AD. Our data offers additional insights into the neurodevelopmental mechanisms of the parietal lobe in AD, highlighting the significant role played by the AG in the disease process.

Abbreviations

MCI, mild cognitive impairment; EMCI, early mild cognitive impairment; LMCI, late mild cognitive impairment; SPL, superior parietal lobule; IPL, inferior parietal lobule; Pcun, precuneus; PoG, postcentral Gyrus; ADNI, Alzheimer's Disease Neuroimaging Initiative; CDR, clinical dementia rating; ADRDA, Alzheimer's Disease and Related Disorders Association; MMSE, Mini-Mental State Examination; ADSC-cog, Alzheimer's Disease Assessment Scale-Cognitive; FAQ, Functional Activities Questionnaire.

Availability of Data and Materials

The authors of this manuscript will make the raw data supporting the conclusions available to any qualified researcher without reservation.

Author Contributions

FL and QM designed the research study and performed the research; FL wrote the original draft; CS and WY provided help and advice on the software and statistical methodology. All authors contributed to editorial changes in the manuscript. All authors have participated sufficiently in the work and agreed to be accountable for all aspects of the work. All authors read and approved the final manuscript.

Ethics Approval and Consent to Participate

The protocol was approved by the Ethics Committee of Affiliated Hospital of North Sichuan Medical College (approval number: 2022ER452-1). The study was carried out in accordance with the guidelines of the Declaration of Helsinki. The patient consent form was waived which was approved by IRB.

Acknowledgment

We are very grateful to the ADNI database and associated researchers for providing us with the data in this study.

Funding

This research received no external funding.

Conflict of Interest

The authors declare no conflict of interest.

Supplementary Material

Supplementary material associated with this article can be found, in the online version, at https://doi.org/10.31083/JIN25991.

References

[1] Pini L, Pievani M, Bocchetta M, Altomare D, Bosco P, Cavedo E, *et al*. Brain atrophy in Alzheimer's Disease and aging. Ageing Research Reviews. 2016; 30: 25–48.

[2] Atri A. The Alzheimer's Disease Clinical Spectrum: Diagnosis and Management. The Medical Clinics of North America. 2019; 103: 263–293.

[3] 2024 Alzheimer's disease facts and figures n.d. Alzheimers Dement. 2024; 20: 3708–3821.

[4] Petersen RC, Roberts RO, Knopman DS, Boeve BF, Geda YE, Ivnik RJ, *et al*. Mild cognitive impairment: ten years later. Archives of Neurology. 2009; 66: 1447–1455.

[5] Ma Z, Jing B, Li Y, Yan H, Li Z, Ma X, *et al*. Identifying Mild Cognitive Impairment with Random Forest by Integrating Multiple MRI Morphological Metrics. Journal of Alzheimer's Disease: JAD. 2020; 73: 991–1002.

[6] Petersen RC. Mild cognitive impairment as a diagnostic entity. Journal of Internal Medicine. 2004; 256: 183–194.

[7] Bennett DA, Wilson RS, Schneider JA, Evans DA, Beckett LA, Aggarwal NT, *et al*. Natural history of mild cognitive impairment in older persons. Neurology. 2002; 59: 198–205.

[8] Femir-Gurtuna B, Kurt E, Ulasoglu-Yildiz C, Bayram A, Yildirim E, Soncu-Buyukiscan E, *et al*. White-matter changes in early and late stages of mild cognitive impairment. Journal of Clinical Neuroscience: Official Journal of the Neurosurgical Society of Australasia. 2020; 78: 181–184.

[9] Cai S, Huang L, Zou J, Jing L, Zhai B, Ji G, *et al*. Changes in thalamic connectivity in the early and late stages of amnestic mild cognitive impairment: a resting-state functional magnetic resonance study from ADNI. PloS One. 2015; 10: e0115573.

[10] Mieling M, Meier H, Bunzeck N. Structural degeneration of the nucleus basalis of Meynert in mild cognitive impairment and Alzheimer's disease - Evidence from an MRI-based meta-analysis. Neuroscience and Biobehavioral Reviews. 2023; 154: 105393.

[11] Möller C, Vrenken H, Jiskoot L, Versteeg A, Barkhof F, Scheltens P, *et al*. Different patterns of gray matter atrophy in early- and late-onset Alzheimer's disease. Neurobiology of Aging. 2013; 34: 2014–2022.

[12] van de Mortel LA, Thomas RM, van Wingen GA, Alzheimer's Disease Neuroimaging Initiative. Grey Matter Loss at Different Stages of Cognitive Decline: A Role for the Thalamus in Developing Alzheimer's Disease. Journal of Alzheimer's Disease: JAD. 2021; 83: 705–720.

[13] Braak H, Braak E. Neuropathological stageing of Alzheimer-related changes. Acta Neuropathologica. 1991; 82: 239–259.

[14] Chen TB, Lai YH, Ke TL, Chen JP, Lee YJ, Lin SY, *et al*. Changes in Plasma Amyloid and Tau in a Longitudinal Study of Normal Aging, Mild Cognitive Impairment, and Alzheimer's Disease. Dementia and Geriatric Cognitive Disorders. 2019; 48: 180–195.

[15] Qu H, Ge H, Wang L, Wang W, Hu C. Volume changes of hippocampal and amygdala subfields in patients with mild cognitive impairment and Alzheimer's disease. Acta Neurologica Belgica. 2023; 123: 1381–1393.

[16] Roesler R, Parent MB, LaLumiere RT, McIntyre CK. Amygdala-hippocampal interactions in synaptic plasticity and memory formation. Neurobiology of Learning and Memory. 2021; 184: 107490.

[17] Herrero MT, Barcia C, Navarro JM. Functional anatomy of thalamus and basal ganglia. Child's Nervous System: ChNS: Official Journal of the International Society for Pediatric Neurosurgery. 2002; 18: 386–404.

[18] Van der Werf YD, Scheltens P, Lindeboom J, Witter MP, Uylings HBM, Jolles J. Deficits of memory, executive functioning and attention following infarction in the thalamus; a study of 22 cases with localised lesions. Neuropsychologia. 2003; 41: 1330–1344.

[19] Spaniol J, Davidson PSR, Kim ASN, Han H, Moscovitch M, Grady CL. Event-related fMRI studies of episodic encoding and retrieval: meta-analyses using activation likelihood estimation. Neuropsychologia. 2009; 47: 1765–1779.

[20] de Flores R, La Joie R, Chételat G. Structural imaging of hippocampal subfields in healthy aging and Alzheimer's disease. Neuroscience. 2015; 309: 29–50.

[21] Shah SN, Dounavi ME, Malhotra PA, Lawlor B, Naci L, Koychev I, *et al*. Dementia risk and thalamic nuclei volumetry in healthy midlife adults: the PREVENT Dementia study. Brain Communications. 2024; 6: fcae046.

[22] He P, Qu H, Cai M, Liu W, Gu X, Ma Q. Structural Alteration of Medial Temporal Lobe Subfield in the Amnestic Mild Cognitive Impairment Stage of Alzheimer's Disease. Neural Plasticity. 2022; 2022: 8461235.

[23] Khan W, Westman E, Jones N, Wahlund LO, Mecocci P, Vellas B, *et al*. Automated Hippocampal Subfield Measures as Predictors of Conversion from Mild Cognitive Impairment to Alzheimer's Disease in Two Independent Cohorts. Brain Topography. 2015; 28: 746–759.

[24] Padulo C, Sestieri C, Punzi M, Picerni E, Chiacchiaretta P, Tullo MG, *et al*. Atrophy of specific amygdala subfields in subjects

converting to mild cognitive impairment. Alzheimer's & Dementia (New York, N. Y.). 2023; 9: e12436.
[25] Censi S, Sestieri C, Punzi M, Delli Pizzi A, Ferretti A, Gambi F, *et al*. "Back to Braak": Role of Nucleus Reuniens and Subcortical Pathways in Alzheimer's Disease Progression. The Journal of Prevention of Alzheimer's Disease. 2024; 11: 1030–1040.
[26] Cabeza R. Role of parietal regions in episodic memory retrieval: the dual attentional processes hypothesis. Neuropsychologia. 2008; 46: 1813–1827.
[27] van Kempen J, Brandt C, Distler C, Bellgrove MA, Thiele A. Dopamine influences attentional rate modulation in Macaque posterior parietal cortex. Scientific Reports. 2022; 12: 6914.
[28] Bogler C, Zangrossi A, Miller C, Sartori G, Haynes JD. Have you been there before? Decoding recognition of spatial scenes from fMRI signals in precuneus. Human Brain Mapping. 2024; 45: e26690.
[29] Wu Z, Peng Y, Hong M, Zhang Y. Gray Matter Deterioration Pattern During Alzheimer's Disease Progression: A Regions-of-Interest Based Surface Morphometry Study. Frontiers in Aging Neuroscience. 2021; 13: 593898.
[30] Hänggi J, Streffer J, Jäncke L, Hock C. Volumes of lateral temporal and parietal structures distinguish between healthy aging, mild cognitive impairment, and Alzheimer's disease. Journal of Alzheimer's Disease: JAD. 2011; 26: 719–734.
[31] Ahulló-Fuster MA, Ortiz T, Varela-Donoso E, Nacher J, Sánchez-Sánchez ML. The Parietal Lobe in Alzheimer's Disease and Blindness. Journal of Alzheimer's Disease. 2022; 89: 1193–1202.
[32] Bayram E, Caldwell JZK, Banks SJ. Current understanding of magnetic resonance imaging biomarkers and memory in Alzheimer's disease. Alzheimer's & Dementia (New York, N. Y.). 2018; 4: 395–413.
[33] Choi Y, Yoon BN, Choi SH, Lim MK, Kim HJ, Yang DW. Reduced Gray Matter Volume in Subjective Cognitive Decline: A Voxel-Based Morphometric Study. Dementia and Neurocognitive Disorders. 2015; 14: 143–148.
[34] Yin C, Yi L, Jia L, Wang J, Liu P, Guo Y, *et al*. Early morphological brain abnormalities in patients with amnestic mild cognitive impairment. Translational Neuroscience. 2014; 5: 253–259.
[35] Mitolo M, Stanzani-Maserati M, Capellari S, Testa C, Rucci P, Poda R, *et al*. Predicting conversion from mild cognitive impairment to Alzheimer's disease using brain ^{1}H-MRS and volumetric changes: A two- year retrospective follow-up study. NeuroImage. Clinical. 2019; 23: 101843.
[36] Qi Z, Wu X, Wang Z, Zhang N, Dong H, Yao L, *et al*. Impairment and compensation coexist in amnestic MCI default mode network. NeuroImage. 2010; 50: 48–55.
[37] Rushworth MFS, Behrens TEJ, Johansen-Berg H. Connection patterns distinguish 3 regions of human parietal cortex. Cerebral Cortex (New York, N.Y.: 1991). 2006; 16: 1418–1430.
[38] Velioglu HA, Hanoglu L, Bayraktaroglu Z, Toprak G, Guler EM, Bektay MY, *et al*. Left lateral parietal rTMS improves cognition and modulates resting brain connectivity in patients with Alzheimer's disease: Possible role of BDNF and oxidative stress. Neurobiology of Learning and Memory. 2021; 180: 107410.
[39] Lattanzio L, Seames A, Holden SK, Buard I. The emergent relationship between temporoparietal junction and anosognosia in Alzheimer's disease. Journal of Neuroscience Research. 2021; 99: 2091–2096.
[40] Yang X, Wu H, Song Y, Chen S, Ge H, Yan Z, *et al*. Functional MRI-specific alterations in frontoparietal network in mild cognitive impairment: an ALE meta-analysis. Frontiers in Aging Neuroscience. 2023; 15: 1165908.
[41] Ma HR, Sheng LQ, Pan PL, Wang GD, Luo R, Shi HC, *et al*. Cerebral glucose metabolic prediction from amnestic mild cognitive impairment to Alzheimer's dementia: a meta-analysis. Translational Neurodegeneration. 2018; 7: 9.
[42] Caminiti SP, De Francesco S, Tondo G, Galli A, Redolfi A, Perani D, *et al*. FDG-PET markers of heterogeneity and different risk of progression in amnestic MCI. Alzheimer's & Dementia: the Journal of the Alzheimer's Association. 2024; 20: 159–172.
[43] Schroeter ML, Stein T, Maslowski N, Neumann J. Neural correlates of Alzheimer's disease and mild cognitive impairment: a systematic and quantitative meta-analysis involving 1351 patients. NeuroImage. 2009; 47: 1196–1206.
[44] Chen Z, Chen K, Li Y, Geng D, Li X, Liang X, *et al*. Structural, static, and dynamic functional MRI predictors for conversion from mild cognitive impairment to Alzheimer's disease: Inter-cohort validation of Shanghai Memory Study and ADNI. Human Brain Mapping. 2024; 45: e26529.
[45] Jacobs HIL, Van Boxtel MPJ, Uylings HBM, Gronenschild EHBM, Verhey FR, Jolles J. Atrophy of the parietal lobe in preclinical dementia. Brain and Cognition. 2011; 75: 154–163.
[46] Fan L, Li H, Zhuo J, Zhang Y, Wang J, Chen L, *et al*. The Human Brainnetome Atlas: A New Brain Atlas Based on Connectional Architecture. Cerebral Cortex (New York, N.Y.: 1991). 2016; 26: 3508–3526.
[47] Paxinos G. Human brainnetome atlas: a new chapter of brain cartography. Science China Life Sciences. 2016; 59: 965–967.
[48] Pievani M, Rasser PE, Galluzzi S, Benussi L, Ghidoni R, Sabattoli F, *et al*. Mapping the effect of APOE epsilon4 on gray matter loss in Alzheimer's disease in vivo. NeuroImage. 2009; 45: 1090–1098.
[49] Gaser C, Dahnke R, Thompson PM, Kurth F, Luders E, The Alzheimer's Disease Neuroimaging Initiative. CAT: a computational anatomy toolbox for the analysis of structural MRI data. Gigascience. 2024; 13: giae049.
[50] Sobie EA. An introduction to MATLAB. Science Signaling. 2011; 4: tr7.
[51] Shi C, Deng H, Deng X, Rao D, Yue W. The Structural Changes of Frontal Subregions and Their Correlations with Cognitive Impairment in Patients with Alzheimer's Disease. Journal of Integrative Neuroscience. 2023; 22: 99.
[52] O'Connor BP. SPSS and SAS programs for determining the number of components using parallel analysis and velicer's MAP test. Behav Res Methods Instrum Comput. 2000; 32: 396–402.
[53] Hoffmann M. The human frontal lobes and frontal network systems: an evolutionary, clinical, and treatment perspective. ISRN Neurology. 2013; 2013: 892459.
[54] Dziedzic TA, Bala A, Marchel A. Cortical and Subcortical Anatomy of the Parietal Lobe From the Neurosurgical Perspective. Frontiers in Neurology. 2021; 12: 727055.
[55] Ahulló-Fuster MA, Ortiz T, Varela-Donoso E, Nacher J, Sánchez-Sánchez ML. The Parietal Lobe in Alzheimer's Disease and Blindness. Journal of Alzheimer's Disease: JAD. 2022; 89: 1193–1202.
[56] Merlo S, Spampinato SF, Sortino MA. Early compensatory responses against neuronal injury: A new therapeutic window of opportunity for Alzheimer's Disease? CNS Neuroscience & Therapeutics. 2019; 25: 5–13.
[57] Stern Y, Barnes CA, Grady C, Jones RN, Raz N. Brain reserve, cognitive reserve, compensation, and maintenance: operationalization, validity, and mechanisms of cognitive resilience. Neurobiology of Aging. 2019; 83: 124–129.
[58] Leng F, Hinz R, Gentleman S, Hampshire A, Dani M, Brooks DJ, *et al*. Neuroinflammation is independently associated with brain network dysfunction in Alzheimer's disease. Molecular Psychiatry. 2023; 28: 1303–1311.
[59] Bradburn S, Murgatroyd C, Ray N. Neuroinflammation in mild cognitive impairment and Alzheimer's disease: A meta-

analysis. Ageing Research Reviews. 2019; 50: 1–8.
[60] McDonald CR, McEvoy LK, Gharapetian L, Fennema-Notestine C, Hagler DJ, Jr, Holland D, *et al*. Regional rates of neocortical atrophy from normal aging to early Alzheimer disease. Neurology. 2009; 73: 457–465.
[61] Misra C, Fan Y, Davatzikos C. Baseline and longitudinal patterns of brain atrophy in MCI patients, and their use in prediction of short-term conversion to AD: results from ADNI. NeuroImage. 2009; 44: 1415–1422.
[62] Seghier ML. The angular gyrus: multiple functions and multiple subdivisions. The Neuroscientist: a Review Journal Bringing Neurobiology, Neurology and Psychiatry. 2013; 19: 43–61.
[63] Jacobs HIL, Van Boxtel MPJ, Jolles J, Verhey FRJ, Uylings HBM. Parietal cortex matters in Alzheimer's disease: an overview of structural, functional and metabolic findings. Neuroscience and Biobehavioral Reviews. 2012; 36: 297–309.
[64] Zhang J, Liu Y, Lan K, Huang X, He Y, Yang F, *et al*. Gray Matter Atrophy in Amnestic Mild Cognitive Impairment: A Voxel-Based Meta-Analysis. Frontiers in Aging Neuroscience. 2021; 13: 627919.
[65] Niu M, Palomero-Gallagher N. Architecture and connectivity of the human angular gyrus and of its homolog region in the macaque brain. Brain Structure & Function. 2023; 228: 47–61.
[66] Li Y, Wang X, Li Y, Sun Y, Sheng C, Li H, *et al*. Abnormal Resting-State Functional Connectivity Strength in Mild Cognitive Impairment and Its Conversion to Alzheimer's Disease. Neural Plasticity. 2016; 2016: 4680972.
[67] Coughlin DG, Hiniker A, Peterson C, Kim Y, Arezoumandan S, Giannini L, *et al*. Digital Histological Study of Neocortical Grey and White Matter Tau Burden Across Tauopathies. Journal of Neuropathology and Experimental Neurology. 2022; 81: 953–964.
[68] Resende EDPF, Hornberger M, Guimarães HC, Gambogi LB, Mariano LI, Teixeira AL, *et al*. Different patterns of gray matter atrophy in behavioral variant frontotemporal dementia with and without episodic memory impairment. International Journal of Geriatric Psychiatry. 2021; 36: 1848–1857.
[69] Rockland KS, Graves WW. The angular gyrus: a special issue on its complex anatomy and function. Brain Structure & Function. 2023; 228: 1–5.
[70] Mizrahi T, Axelrod V. Similarity in activity and laterality patterns in the angular gyrus during autobiographical memory retrieval and self-referential processing. Brain Structure & Function. 2023; 228: 219–238.
[71] Güntürkün O, Ströckens F, Ocklenburg S. Brain Lateralization: A Comparative Perspective. Physiological Reviews. 2020; 100: 1019–1063.
[72] Thompson PM, Hayashi KM, de Zubicaray G, Janke AL, Rose SE, Semple J, *et al*. Dynamics of gray matter loss in Alzheimer's disease. The Journal of Neuroscience: the Official Journal of the Society for Neuroscience. 2003; 23: 994–1005.
[73] Wachinger C, Salat DH, Weiner M, Reuter M, Alzheimer's Disease Neuroimaging Initiative. Whole-brain analysis reveals increased neuroanatomical asymmetries in dementia for hippocampus and amygdala. Brain: a Journal of Neurology. 2016; 139: 3253–3266.
[74] Pennanen C, Testa C, Laakso MP, Hallikainen M, Helkala EL, Hänninen T, *et al*. A voxel based morphometry study on mild cognitive impairment. Journal of Neurology, Neurosurgery, and Psychiatry. 2005; 76: 11–14.
[75] Shi F, Liu B, Zhou Y, Yu C, Jiang T. Hippocampal volume and asymmetry in mild cognitive impairment and Alzheimer's disease: Meta-analyses of MRI studies. Hippocampus. 2009; 19: 1055–1064.
[76] Frings L, Hellwig S, Spehl TS, Bormann T, Buchert R, Vach W, *et al*. Asymmetries of amyloid-β burden and neuronal dysfunction are positively correlated in Alzheimer's disease. Brain: a Journal of Neurology. 2015; 138: 3089–3099.
[77] Tetzloff KA, Graff-Radford J, Martin PR, Tosakulwong N, Machulda MM, Duffy JR, *et al*. Regional Distribution, Asymmetry, and Clinical Correlates of Tau Uptake on [18F]AV-1451 PET in Atypical Alzheimer's Disease. Journal of Alzheimer's Disease. 2018; 62: 1713–1724.
[78] Punzi M, Sestieri C, Picerni E, Chiarelli AM, Padulo C, Delli Pizzi A, *et al*. Atrophy of hippocampal subfields and amygdala nuclei in subjects with mild cognitive impairment progressing to Alzheimer's disease. Heliyon. 2024; 10: e27429.